

Spin waves in disordered FeCo magnonic crystal at finite temperatures

Sebastian Paischer,^{1,*} Paweł A. Buczek,² Nadine Buczek,³ David Eilmsteiner,¹ and Arthur Ernst^{4,1}

¹*Institute for Theoretical Physics, Johannes Kepler University Linz, Altenberger Straße 69, 4040 Linz*

²*Department of Engineering and Computer Sciences,*

Hamburg University of Applied Sciences, Berliner Tor 7, 20099 Hamburg, Germany

³*Department of Applied Natural Sciences, Lübeck University of Applied Sciences, Mönkhofer Weg 239, 23562 Lübeck, Germany*

⁴*Max-Planck-Institut of Microstructure Physics, Weinberg 2, 06120 Halle (Saale), Germany*

(Dated: May 24, 2022)

We study theoretically the influence of the temperature and disorder on the spin wave spectrum of the magnonic crystal $\text{Fe}_x\text{Co}_{1-x}$. Our formalism is based on the analysis of Heisenberg Hamiltonian with the exchange integrals obtained from the *ab initio* magnetic force theorem by means of wave vector and frequency dependent transverse magnetic susceptibility. The coherent potential approximation is employed to treat the disorder and random phase approximation in order to account for the softening of the magnon spectrum at finite temperatures. The alloy turns out to exhibit many advantageous properties for spintronic applications. Apart from high Curie temperature, its magnonic bandgap remains stable at elevated temperatures and is largely unaffected by the disorder. We pay particular attention to the attenuation of magnons introduced by the alloying. The damping turns out to be a non-monotonic function of the impurity concentration due to the non-trivial evolution of exchange integrals with the Co concentration. The disorder induced damping of magnons is estimated to be much smaller than their Landau damping.

I. INTRODUCTION

Magnon spintronics, or magnonics, is a novel promising strategy in the engineering of data processors [1]. It takes advantage of spin waves (also called magnons) in order to perform logical computations [2, 3]. Magnons emerge as collective excitations of magnetically ordered solids and can be pictured as wave-like coherent precession of atomic moments [4]. In periodic structures, including atomic lattices, these quasiparticles are Bloch waves, carrying energy and crystal momentum. Magnonic computers avoid numerous drawbacks of classical semiconductor based computers, but they rely heavily on suitably designed magnon propagation media. Their particularly relevant class are *magnonic crystals* [5, 6] featuring spin wave propagation properties not typically found in common magnetic solids like elemental ferro- and antiferromagnets, especially the emergence of a *magnonic gap*, i.e. frequency bands in which magnon states cannot propagate in the solid [7, 8]. This feature, combined with the unique spin wave dispersion close to the band edges, provides a rich toolbox for magnon mode engineering, including the possibility of selective spin wave excitations and propagation, magnon mode confinement and deceleration, and bandgap soliton generation [9–11].

The bulk of the current research in this domain revolves around the utilization of long wave-length magnons with energies in the gigahertz band. Nevertheless, in order to definitely push the size and speed limits of modern semiconductor computers, one must resort to the spin waves in the terahertz regime. While the foundations for the magnonic information processing in the terahertz regime are laid, the potential of the

terahertz magnonics remains vastly unexplored [12]. At the same time, one expects well defined spin waves in this energy range [13] and in systems with many different atoms in the primitive cell, the modes may well arrange in bands separated by the magnonic gap [14], yielding natural magnonic crystals.

Here, we concentrate on the ferromagnetic $\text{Fe}_x\text{Co}_{1-x}$ alloy. With typical magnon energies well within the terahertz range, a high Curie temperature [15, 16] and the bandgap in the spectrum, opening due to the large difference in the interaction strengths and magnetic moments of the constituents and remaining stable at elevated temperatures, the alloy family shows all the necessary properties for a terahertz magnonic crystals. It is interesting to note that the magnonic crystals used in terahertz applications are typically artificial heterostructures obtained from elaborate fabrication processes. On the contrary, in the terahertz range, the natural microscopic arrangement of atoms in alloys like $\text{Fe}_x\text{Co}_{1-x}$ would suffice to create cheap magnonic crystals.

In metals, the life-time of the modes can be severely limited by the interaction of these collective modes with the single particle continuum, called Landau damping [17–19], but means of viable engineering of long-living magnons have been proposed, such as reducing the system's dimensionality and alloying [20]. The latter method leads to a further momentum dissipation mechanism, in which the Bloch waves cease to be the eigenstates of the magnetic Heisenberg-like Hamiltonian and acquire a finite lifetime arising from the scattering on the crystal imperfections [21, 22]. This picture of the weak attenuation might break down if the magnon spectra become dominated by strongly spatially localized modes. Further mechanism limiting the life-time of the magnon modes, and thus their potential to propagate dissipationlessly through the medium, is the interaction of the modes with

* sebastian.paischer@jku.at

a thermal bath.

Solids, and in particular nanostructures, often feature structural imperfections. Furthermore, in order to be usable, the magnonic computers must be able to operate at and typically well above room temperature. Thus, it is prudent to delve into the central question of this paper, namely how the magnonic properties evolve in real, imperfect or alloyed solids at non-zero temperatures. We show that the increase of the disorder in $\text{Fe}_x\text{Co}_{1-x}$ alloy not only preserves the magnonic gap but can even be used to precisely engineer its value and further properties.

Among others, we address the influence of temperature and disorder on the magnonic band gap as well as on the dispersion and life-times of the spin waves. Our formalism is based on the coherent potential approximation (CPA) applied to the disordered Heisenberg ferromagnet [21]. The superiority of our method compared to other treatments of the same problem is the possibility to account for complex crystal structures. To incorporate finite temperature effects, we implemented a modified version of the random phase approximation (RPA) discussed in reference [23]. Our formalism does not include the Landau damping of the spin waves. This attenuation mechanism can be pronounced in metallic magnonic crystals and can be described within the framework of many-body perturbation theory [24] or time-dependent density functional theory [18]. Unfortunately, at the moment, there is no feasible formal and computational methodology allowing to incorporate the effects of disorder or temperature into these two approaches.

The paper is organized as follows: In chapter II, the theoretical background of the RPA-CPA theory for the disordered Heisenberg ferromagnet is discussed. Some numerical details are given in section III. The results are presented in chapter IV.

II. THEORY

The Heisenberg ferromagnet is characterized by the Hamiltonian

$$H = -\frac{1}{2} \sum_{i,j} J_{ij} \mathbf{e}_i \cdot \mathbf{e}_j \quad (1)$$

where J_{ij} are the exchange parameters which can be obtained from the magnetic force theorem [25] and \mathbf{e}_i is a unit vector in the direction of the magnetic moment. To calculate magnon-properties, the transverse susceptibility [26]

$$\chi_{ij}(t, t') = -i \Theta(t - t') \overline{[\mu_i^+(t), \mu_j^-(t')]} \quad (2)$$

with $\mu_i^\pm = \mu_i^x \pm i\mu_i^y$, μ_i^α being the α -component of the magnetic moment $\boldsymbol{\mu}_i$ on the lattice site i and the overline represents a thermal average, is computed. The corre-

sponding equation of motion reads

$$z\chi_{ij}(z) = 2g\delta_{ij} \bar{\mu}_i - g \sum_{\ell} \frac{\bar{\mu}_i}{\mu_i \mu_{\ell}} J_{i\ell} \chi_{\ell j}(z) + g \sum_{\ell} \frac{\bar{\mu}_{\ell}}{\mu_i \mu_{\ell}} J_{i\ell} \chi_{ij}(z). \quad (3)$$

with the electron Landé factor g and the energy $z = E + i\varepsilon$. The disorder is modeled by defining occupation variables

$$p^{i\alpha}(\mathbf{R}) = \begin{cases} 1 & \text{species } \alpha \text{ on basis site } i \text{ in unit cell } \mathbf{R} \\ 0 & \text{else} \end{cases} \quad (4)$$

and a species resolved Fourier transformation of the susceptibility

$$\chi_{ij}^{\alpha\beta}(\mathbf{k}, \mathbf{k}') := \sum_{\mathbf{R}, \mathbf{R}'} p^{i\alpha}(\mathbf{R}) e^{-i\mathbf{k} \cdot \mathbf{R}} \chi_{ij}(\mathbf{R}, \mathbf{R}') p^{j\beta}(\mathbf{R}') e^{i\mathbf{k}' \cdot \mathbf{R}'}. \quad (5)$$

In the following, it is useful to introduce a combined site and species index denoted by $(i) = i\alpha$, $(j) = j\beta$, etc.. Writing the susceptibility given in formula (3) as a series and performing the Fourier transformation (equation (5)) leads to expressions with products of Fourier transformed occupation variables

$$\varrho^{(i)}(\mathbf{k}) = \sum_{\mathbf{R}} p^{(i)}(\mathbf{R}) e^{-i\mathbf{k} \cdot \mathbf{R}}. \quad (6)$$

The averaging process needs to be done very carefully as described in references [21] and [27] and leads to the appearance of cumulants of order n given by

$$\mathcal{C}_{(\ell_1)(\ell_2)\dots(\ell_n)}^n(\mathbf{k}_1, \mathbf{k}_2 \dots \mathbf{k}_n) = \mathcal{P}_{(\ell_1)(\ell_2)\dots(\ell_n)}^n(\mathbf{c}) \cdot \Omega_{\text{BZ}} \delta(\mathbf{k}_1 + \mathbf{k}_2 + \dots + \mathbf{k}_n) \quad (7)$$

where \mathbf{c} is a matrix with the concentrations of each species on the sublattices and the weight functions $\mathcal{P}_{(\ell_1)(\ell_2)\dots(\ell_n)}^n(\mathbf{c})$. There is no analytic representation of the latter but the first two are given by

$$\begin{aligned} \mathcal{P}_{(i)}^1 &= c^{(i)} \\ \mathcal{P}_{(i)(j)}^2 &= \delta_{ij}(\delta_{\alpha\beta} c^{(i)} - c^{(i)} c^{(j)}). \end{aligned} \quad (8)$$

A summary of the resulting formulae after the Fourier transformation and the averaging can be found in figure 1 in diagrammatic form where the following symbols have been used:

- The τ -matrix

$$\begin{aligned} \tau_{(i)(j)}^{(\ell)}(\mathbf{k}, \mathbf{k}') &= g\mu_{(j)}^{-1} \left(J_{(j)(\ell)}(\mathbf{k} - \mathbf{k}') \frac{\bar{\mu}_{(\ell)}}{\mu_{(\ell)}} \delta_{(i)(j)} \right. \\ &\quad \left. - J_{(\ell)(j)}(\mathbf{k}') \frac{\bar{\mu}_{(i)}}{\mu_{(i)}} \delta_{(i)(\ell)} \right) \end{aligned} \quad (9)$$

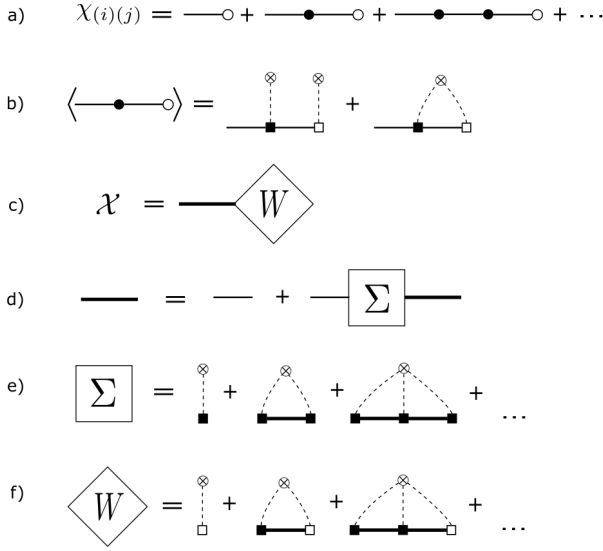


Figure 1. Diagrammatic representation of the main results of the CPA-theory. a) Fourier transformation of series (3), b) average of the second term in a), c) the averaged susceptibility \mathcal{X} written as a product of the effective medium propagator Ξ (thick line) and the spin weight W , d) Dyson equation for the effective medium propagator, e) definition of the self-energy Σ and f) definition of the spin weight W

where

$$J_{(i)(j)}(\mathbf{k}) = \sum_{\mathbf{R}} J_{(i)(j)}(\mathbf{R}) e^{-i\mathbf{k} \cdot \mathbf{R}} \quad (10)$$

is represented by a filled square.

- The filled circle represents a T - matrix

$$T_{(i)(j)}(\mathbf{k}, \mathbf{k}') = \sum_{(\ell)} \varrho^{(\ell)}(\mathbf{k} - \mathbf{k}') \tau_{(i)(j)}^{(\ell)}(\mathbf{k}, \mathbf{k}'). \quad (11)$$

- An empty square stands for a σ -matrix:

$$\sigma_{(i)(j)}^{(\ell)} = 2g\delta_{(i)(j)}\delta_{(i)(\ell)}\bar{\mu}_{(\ell)} \quad (12)$$

- The S -matrix is depicted as an empty circle and is given by

$$S_{(i)(j)}(\mathbf{k}, \mathbf{k}') = \sum_{(\ell)} \varrho^{(\ell)}(\mathbf{k} - \mathbf{k}') \sigma_{(i)(j)}^{(\ell)}. \quad (13)$$

- The propagator of uncoupled magnetic moments, represented by a solid line, is given as

$$\Gamma_{(i)(j)}(z) = z^{-1}\delta_{(i)(j)}. \quad (14)$$

- A cumulant of order n is represented by a crossed circle, where the order is given by the number of dashed lines ending at it.

Furthermore, two rules for the interpretation of the diagrams need to be followed:

1. The elements brought together in a diagram undergo a matrix multiplication in the $(i)(j)$ -space. The corresponding matrix indices are written as subscripts in the definitions above.
2. Every internal free propagator is assigned a momentum which is integrated over:

$$\frac{1}{\Omega_{\text{BZ}}} \int_{\Omega_{\text{BZ}}} d^3k_1 \quad (15)$$

Every term of the series for the susceptibility in figure 1 a) is averaged independently. The result for the second term is shown in figure 1 b). In the CPA, crossed terms, which appear in the fourth and higher order terms, are neglected. This model represents a single-site approximation and neglects all correlations between two or more sites. As these averaged diagrams consist of two different vertices (filled and empty squares), the averaged susceptibility can be written as a product of two different contributions which we call the effective medium propagator Ξ and the spin weight W as is shown in figure 1 c). The effective medium propagator is given in terms of a Dyson-equation shown in figure 1 d) with a self-energy defined in figure 1 e). Together with the definition of the spin-weight in figure 1 f), all non-crossed diagrams of the averaged susceptibility can be constructed.

The calculation of the self-energy is done through the partial self-energies defined by

$$c^{i\alpha} \hat{\Sigma}^{i\alpha} = \mathcal{P}_{i\alpha}^1 \mathbb{1} + \mathcal{P}_{i\beta, i\alpha}^2 M^{i\beta} + \mathcal{P}_{i\gamma, i\beta, i\alpha}^3 M^{i\gamma} M^{i\beta} + \dots \quad (16)$$

where the M -matrix is given by

$$M^{(i)}(z, \mathbf{k}, \mathbf{k}') = \tau^{(i)}(\mathbf{k}, \mathbf{k}') \Xi(z, \mathbf{k}'). \quad (17)$$

With that the self-energy is given by

$$\Sigma(z, \mathbf{R}, \mathbf{R}') = \sum_{(i)} c^{(i)} \sum_{\mathbf{R}_1} \hat{\Sigma}^{(i)}(z, \mathbf{R}, \mathbf{R}_1) \tau^{(i)}(\mathbf{R}_1, \mathbf{R}') \quad (18)$$

which can also be seen through its diagrammatic definition. The self-consistency equation inspired by the works of [27] and [28] is given by

$$\hat{\Sigma}^{(i)} = \left[\mathbb{1} - \left(M^{(i)} - \bar{\Sigma}^{(i)} \right) \right]^{-1} \quad (19)$$

where the helping quantity

$$\bar{\Sigma}^i(\mathbf{R}, \mathbf{R}') = \sum_{\alpha \in I_i} \sum_{\mathbf{R}_1} c_{i\alpha} \hat{\Sigma}^{i\alpha}(\mathbf{R}, \mathbf{R}_1) M^{i\alpha}(\mathbf{R}_1, \mathbf{R}'). \quad (20)$$

is used. Equation (19) is used to calculate a new self-energy from the effective medium propagator with which

through figure 1 c) a new effective medium propagator can be calculated.

The temperature dependence is calculated through the average magnon number

$$\Phi_{(i)} = \text{Im} \left\{ \int_{-\infty}^{\infty} dz \frac{D_{(i)}(z)}{e^{\frac{z}{k_B T}} - 1} \right\} \quad (21)$$

where

$$D_{(i)}(z) = -\frac{1}{\pi} \int_{\Omega_{\text{BZ}}} d^3k \frac{\mathcal{X}_{(i)(i)}(z, \mathbf{k})}{2gc_{(i)}\bar{\mu}_{(i)}}. \quad (22)$$

Note that the imaginary part of this quantity $D_{(i)}(z)$ is the magnonic density of states. Following the theory of Callen [23] and its implementations in simple disordered and complex ordered systems [29–31], the thermally averaged magnetic moments are

$$\bar{\mu}_{(i)} = g \frac{\left(\frac{\mu_{(i)}}{g} - \Phi_{(i)}\right)(1 + \Phi_{(i)})^{\mu_{(i)}+1} + \left(\frac{\mu_{(i)}}{g} + 1 + \Phi_{(i)}\right)\Phi_{(i)}^{\mu_{(i)}+1}}{(1 + \Phi_{(i)})^{\mu_{(i)}+1} - (\Phi_{(i)})^{\mu_{(i)}+1}}. \quad (23)$$

III. IMPLEMENTATION

The integrals in \mathbf{k} -space (see equation (22)) were computed using the tetrahedron method [32]. The energy integral is problematic as $D_{(i)}(z)$ is a rapidly changing function along the real axis and in addition to that the Bose-factor $\frac{1}{e^{\frac{z}{k_B T}} - 1}$ has a pole at $z = 0$. Therefore, the energy-integral was implemented using complex contour integration. The problem was tackled by calculating two complex integrals, which are shown in figure 2. C is a semi-circle with radius z_{MAX} and C' is a closed contour consisting of the same arc as C but in the opposite direction and a straight line infinitesimally close to the real axis. The closed contour C' was evaluated using the Residue-theorem as the Bose-factor has Poles along the imaginary axis at $z_n = 2n\pi i k_B T$ with $n \in \mathbb{Z}$. The values of the residues are given by

$$R(z_n) = k_B T D_{(i)}(z_n). \quad (24)$$

The sum of both contours C and C' gives the integral parallel and infinitesimally close along the real axis.

This method is based on the fact that the integrand in equation (21) is analytic almost everywhere in the complex upper half plane and on the fact that it vanishes for very large positive and negative energies. The radius of the integration contour z_{MAX} was estimated using the Gersgorin disc theorem [33].

Another complication arises from the fact that the Bose-factor has a singularity at $z = 0$. As mentioned above, the method used here gives the integral parallel

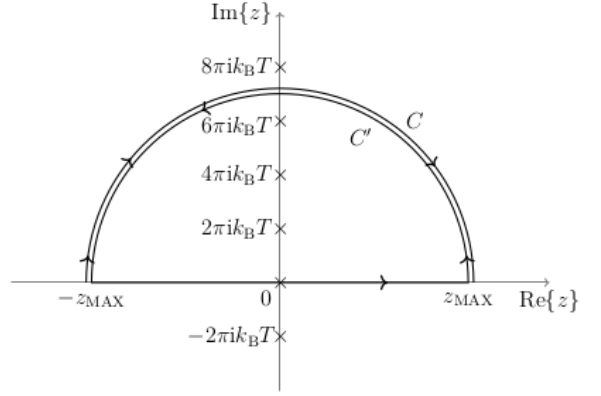


Figure 2. Integration contour used to calculate $\Phi_{(i)}$. The crosses on the imaginary axis mark the poles of $\frac{1}{e^{\frac{z}{k_B T}} - 1}$.

to the real axis at an infinitesimal distance Δ . Therefore the integral calculated through the complex contour integration described above is

$$\Phi_{(i)} = \text{Im} \left\{ \int_{-\infty}^{\infty} \frac{D_{(i)}(E + i\Delta)}{e^{\beta E} - 1 + i\Delta\beta e^{\beta E}} dE \right\} \quad (25)$$

where $e^{\Delta x} \approx 1 + \Delta x$ was used. This can be rewritten using the Shokotski-Plemelj Theorem

$$\lim_{\Delta \rightarrow 0} \frac{1}{x + i\Delta} = \frac{\mathcal{P}}{x} - i\pi\delta(x) \quad (26)$$

where \mathcal{P} is the Cauchy principal value. Now, $\Phi_{(i)}$ is given by the principal value integral but because of the extension of the integration contour, an additional contribution

$$i\pi k_B T D_{(i)}(0) \quad (27)$$

is picked up. This contribution is spurious and needs to be subtracted from the result of the integral.

In the limit $T \rightarrow T_C$, the average magnon number $\Phi_{(i)}$ goes to infinity, which allows a series expansion of equation (23) in $\frac{1}{\Phi_{(i)}}$:

$$\bar{\mu}_{(i)} = \frac{\mu_{(i)}(\mu_{(i)} + g)}{3g\Phi_{(i)}} + \mathcal{O}\left(\left(\frac{1}{\Phi_{(i)}}\right)^2\right) \quad (28)$$

Expanding the exponential in formula (21) and inserting it in the series expansion above leads to

$$\bar{\mu}_{(i)} = -\pi \frac{\mu_{(i)}(\mu_{(i)} + g)}{3gk_B T_C} \left[\int dz \int d^3k \frac{\mathcal{X}_{(i)(i)}(z, \mathbf{k})}{2gc_{(i)}\bar{\mu}_{(i)}z} \right]^{-1}. \quad (29)$$

An important point is that the latter equation still holds if all the averaged magnetic moments are scaled by an

arbitrary constant factor. This fact is obvious in ordered systems as is shown in reference [31] and also holds in substitutionally disordered systems. Using this property, the calculation of the Curie temperature can be done by treating the averaged moments as vector and solving the equation

$$\bar{\mu}_{(i)} = -\pi \frac{\mu_{(i)}(\mu_{(i)} + g)}{3gk_B} \left[\int dz \int d^3k \frac{\mathcal{X}_{(i)(i)}(z, \mathbf{k})}{2gc_{(i)}\bar{\mu}_{(i)}z} \right]^{-1}. \quad (30)$$

iteratively while also normalizing this vector to an arbitrary length in each step. Note that in equation (30) the factor T_C is omitted. After convergence is reached, the Curie temperature is given by the length of the vector.

One of the main advantages of the presented formalism is that the two main parameters entering the model, magnetic moments μ_i^α and exchange constants J_{ij} , can be calculated from first-principles. Thus, our approach in a combination with a density functional theory method provides a parameter free description of spin waves in substitutional magnetic alloys and ordered materials at finite temperatures.

IV. RESULTS

Magnetic moments μ_i^α and exchange parameters J_{ij} of iron-cobalt alloys at various concentrations were evaluated using a first-principles Green-function method within a generalized gradient approximation of density functional theory [34]. The method is designed for bulk materials, surfaces, interfaces and real space clusters [35–37]. Disorder effects were taken into account within a coherent-potential approximation [38] as it is implemented within multiple scattering theory [39]. The exchange interaction was estimated using the magnetic force theorem [25] formulated for substitutional alloys within the CPA approach [40].

We consider the interaction between 12 shells of neighbors. To ensure the convergence of calculated properties with the number of neighbor shells, several calculations were performed for up to 30 shells showing practically the same results as with 12.

For better comparability, all the results were calculated using a bcc-structure. Furthermore, the interaction parameters J_{ij} are held constant (at their value at $T=0K$) while increasing the temperature.

A. Random disorder

1. Curie temperatures

As cobalt has a higher Curie temperature than iron, one would expect a rise of the critical temperature as the concentration of cobalt c is increased. Our results shown

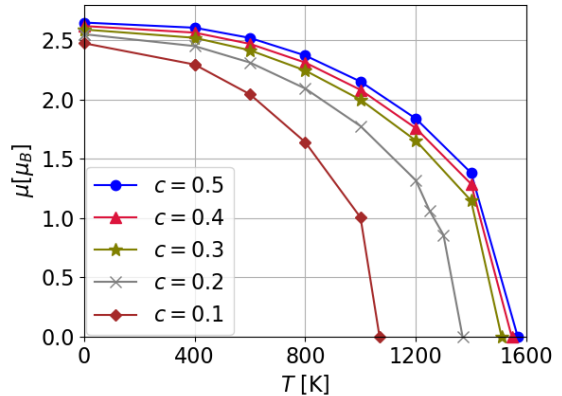


Figure 3. Magnetic moments of iron in $\text{Fe}_{1-c}\text{Co}_c$ for different temperatures and cobalt concentrations. Lines are ment as a guide to the eye.

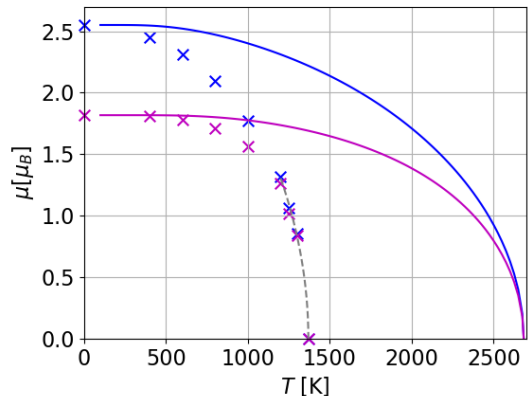


Figure 4. Magnetic moments in $\text{Fe}_{0.8}\text{Co}_{0.2}$ for different temperatures within the RPA (crosses) and the MFA (lines). The blue line represents iron while the red line represents cobalt. The dashed line represents the expected behavior of the Heisenberg model near the Curie temperature.

in figure 3 display this behavior. The points in this figure are the numerical results which were calculated using the methods described in the previous section. Near the magnetic phase transition the characteristic behavior of the averaged magnetic moments is given by

$$\bar{\mu} \propto \left(1 - \frac{T}{T_C}\right)^\beta. \quad (31)$$

The critical exponent β has the numeric value of $1/2$ in the case of the Heisenberg model in the RPA [41], which is well known to differ from the experimental value of $\beta \approx 1/3$ [26]. For the system with $c = 0.2$, we used the latter equation as a fitting function with $\beta = 1/2$ for our results close to T_C . It fits very well with our data, cf. figure 4. Apart from deploying the RPA, we estimated the Curie temperature using the mean-field approximation

c	T_C^{RPA} [K]	T_C^{MFA} [K]	T_C [K] in [16]	T_C [K] in [15]
0.1	1069	2199	1164	1144
0.2	1369	2684	1225	1211
0.3	1510	2844	1260	1243
0.4	1547	2837	1268	1250
0.5	1568	2803	1265	1243

Table I. Comparison of the Curie temperatures calculated in this work with experimental results in [15, 16]

(MFA). The MFA is a purely classical model in which the thermally averaged magnetic moments are given by [26]

$$\bar{\mu}_{(i)} = \mu \cdot B_{\mu_{(i)}} \left(\frac{g\mu_B B_{(i)}^m \mu_{(i)}}{k_B T} \right) \quad (32)$$

with the Bohr magneton μ_B , the Brillouin function $B_\mu(x)$ and the mean field

$$B_{(i)}^m = \frac{1}{\mu_B \mu_{(i)}} \sum_{\mathbf{R}(j)} J_{(i)(j)}(\mathbf{R}) c_{(j)} \frac{\bar{\mu}_{(j)}}{\mu_{(j)}}. \quad (33)$$

While the RPA is known to underestimate the Curie temperature [31], the mean field approximation (MFA) overestimates it. This is caused by the fact that the MFA neglects the influence of magnons and therefore only allows spin flips as elementary excitations, which naturally arises at higher energies than magnons [26]. Thus, the combination of these two methods may be used to provide bounds for the approximate theoretical predictions. The MFA equations can be solved iteratively and yield the results shown in figure 4 for $\text{Fe}_{0.8}\text{Co}_{0.2}$. They are almost twice as large as their RPA counterparts, thus providing rather poor account of the high temperature behavior of the alloy considered.

The results are summarized in table I together with experimental results from references [15, 16]. While RPA performs fairly well, a clear trend to overestimating the Curie temperature can be seen. Partially, the behavior can be attributed to the fact that in our calculations we restrict the system to a bcc-lattice, while the real iron cobalt system will undergo a structural phase transition at elevated temperatures [16] which is expected to influence the Curie temperature.

2. Magnonic spectrum

We extract the magnonic spectrum from the imaginary part of the retarded averaged susceptibility $\chi(q, \omega)$. The most prominent feature is its bandgap appearing due to strongly different interaction strengths and magnetic moments between different constituents. Our results suggest that this bandgap is stable up to high temperatures as can be seen in the result for $\text{Fe}_{0.8}\text{Co}_{0.2}$ presented in figure 5. In the upper (lower) plot the spectrum for the

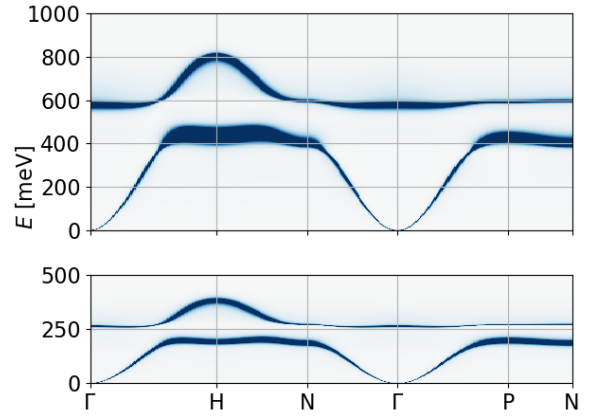


Figure 5. Magnonic spectrum of $\text{Fe}_{0.8}\text{Co}_{0.2}$ at $T=0$ K (top) and $T \approx 0.9 T_C$ (bottom).

case of $T=0$ K ($T \approx 0.9T_C$) is shown. Interestingly, the main features of the band structure are preserved as the temperature increases. The scaling (softening) of the magnonic spectrum proportional to the thermally averaged magnetic moment is a feature of the RPA. In this approximation, the magnon energies vanish above the Curie temperature. In a more sophisticated treatment, the spectrum above the critical temperature should feature paramagnetic like excitations emerging as a manifestation of the short-range magnetic order [42].

Let us note that the peaks feature finite width appearing due to the presence of disorder in the system. The damping is relatively small and increases somewhat only at elevated energies, in particular close to the edges of the bandgap. Within the RPA, the width of the peaks is independent of temperature as can be seen from equation 3.

3. Width of the bandgap, spin stiffness and lifetimes

We investigate the spin wave stiffness constant C describing the quadratic magnon dispersion of the acoustic mode in the long wave-length limit

$$E = Ck^2 \quad (34)$$

as well as the size of the bandgap. Both decrease roughly proportionally to the average magnetization (see figure 6) as the temperature is increased. The reference values at $c=20\%$ and $T=0$ K

$$C_0 \approx 477 \text{ meV \AA}^2 \quad E_G^0 = 115 \text{ meV} \quad (35)$$

are in reasonable agreement with values from other studies of iron and cobalt [17, 43].

Furthermore, we determine the full width at half maximum (FWHM) of the magnon peaks for several wave-vectors. The FWHM is computed using a Lorentzian fit

function for the imaginary part of the susceptibility as function of the energy:

$$\text{Im}\{\chi\}(E) \approx h \frac{\frac{1}{2}\text{FWHM}}{(E - E_0)^2 + (\frac{1}{2}\text{FWHM})^2} \quad (36)$$

with the location of the maximum E_0 of the peak with scaling factor h . The FWHM is interpreted as the inverse magnon lifetime. In order to facilitate a quantitative comparison, we normalize the width to the energy of the magnon for a particular wave-vector. This feature can be interpreted as the inverse of the quality factor, giving the amount of energy leaking from the mode per cycle of the precession.

We recall that in our formalism the finite widths of the magnon resonances arise only due to the action of the disorder. Nevertheless, at constant Co concentration c , the FWHM varies with the temperature as well. In a simple picture, this somewhat unexpected observation can be interpreted as follows: The scattering rate of magnons of particular energy on the crystal imperfections (or alternatively the FWHM for weak coupling) is proportional to the concentration of dopants and the density of final magnon states with this energy, as the scattering potential is static. Even though the density of states decreases with temperature, it does not necessarily retain its shape. Thus, for different modes with different wave-vectors the density of available finite states will vary as the temperature is raised. As evident from figure 7, this effect depends on the magnon state. With rising temperature, the normalized widths increase for low energy acoustic magnons, but decrease for magnons at the top of the acoustic branch and in the optical branch.

However, we note again that our prediction concerning the evolution of the width with the temperature, due to the use of the RPA, does not include the main mechanism, i.e. the coupling of the magnons to the thermal bath. In the RPA, without disorder, the magnons would feature an infinite life-time. In general, it is expected, that the thermally induced width should increase with the temperature [44].

The evolution of the magnonic spectrum with the disorder shows several interesting features. For small Co concentrations, the bandgap increases slightly and above $c \approx 0.1$ starts to decrease with c , cf. figure 6. As mentioned before, in simple terms, the gap arises because of the large difference in the exchange integrals (magnetic interactions) and magnetic moments between different constituents. Figure 9 shows that this difference is pronounced most strongly for low concentrations. The strong increase of the nearest neighbor Fe-Fe interaction as the Co concentration increases causes the bandgap to get narrower, as this exchange integral becomes similar in magnitude to the Co-Co interaction. The enhancement of Fe-Fe exchange interaction with increase of Co concentration can be explained by a strong hybridization between $3d$ states of Fe and Co atoms. In addition, the presence of Co leads to enhancement of the density of states

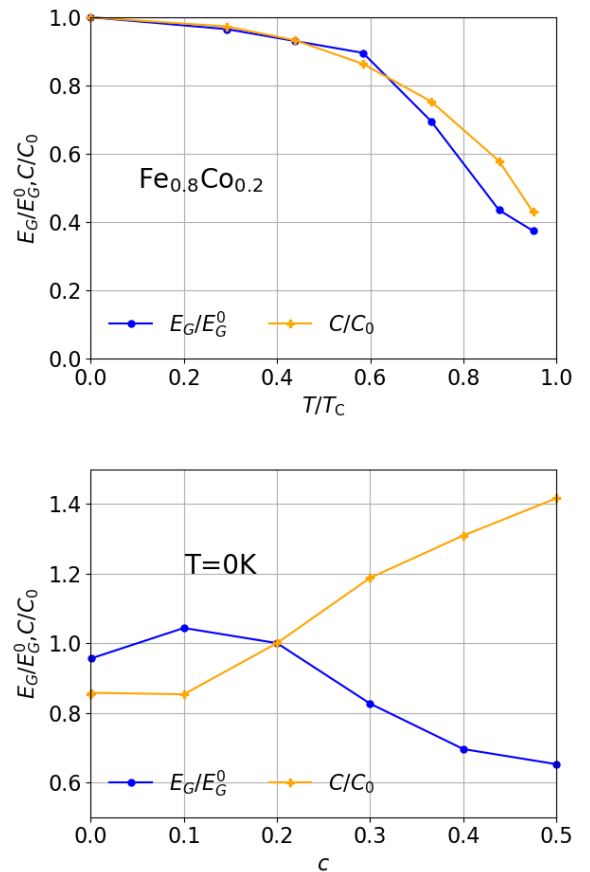


Figure 6. Relative width of the bandgap $\frac{E_G}{E_G^0}$ and relative spin stiffness $\frac{C}{C_0}$ for different Cobalt-concentrations at $T = 0$ K (top) and for different temperatures at $c = 20\%$ (bottom). All quantities are normalized to their values at $c = 20\%$ and $T = 0$ K ($C_0 \approx 477 \text{ meV \AA}^2$, $E_G^0 = 115 \text{ meV}$).

at the Fermi level, increasing the Stoner factor and the exchange interaction. Increase of the Co concentration fills up the bands mainly in the minority spin channel. Fig. 10 shows the calculated Bloch spectral functions for $c = 0.5\%$ and $c = 10\%$ for both majority and minority spin channels, respectively. The most important changes occur along the Γ -H line and in the vicinity of the Γ point. At low Co concentrations a band along the Γ -H is in the Fermi level's vicinity but is not occupied. It is filled up at higher Co concentrations ($c > 5\%$) and leads to a significant increase of the magnetic interaction in the systems. At high cobalt concentrations, it is mainly the difference of the magnetic moments which prevents the closing of the bandgap. To verify this statement we show the spectrum of $\text{Fe}_{0.5}\text{Co}_{0.5}$ with equal magnetic moments for both constituents $\mu_{\text{Fe}} = \mu_{\text{Co}}$. As can be seen in figure 8, the bandgap closes in this case.

Finally, we note that the FWHM shows maxima at certain concentrations, which are caused by the change of the exchange parameters. In figure 11, we show the

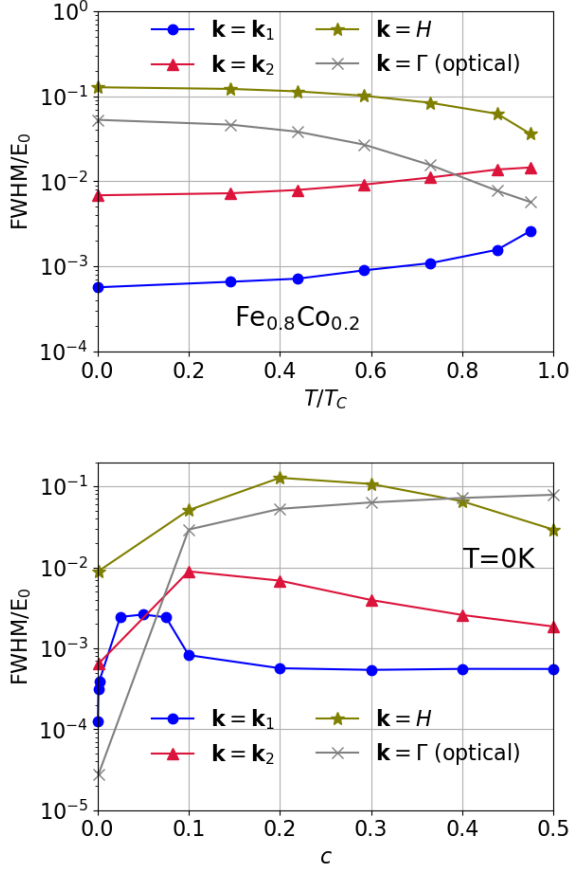


Figure 7. FWHM at $\mathbf{k}_1 = (0.1, 0, 0) \frac{1}{a_B}$, $\mathbf{k}_2 = (0.57, 0, 0) \frac{1}{a_B}$ (midway between Γ and H), H and the optical mode at Γ for different Cobalt-concentrations at $T = 0$ K (bottom) and for different temperatures at $c = 20\%$ (top). All quantities are normalized to their values at $c = 20\%$ and $T = 0$ K.

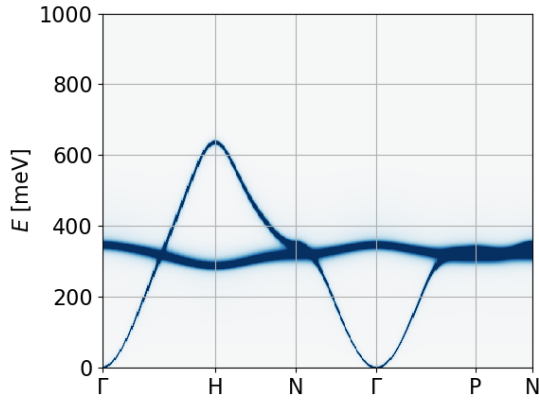


Figure 8. Magnonic spectrum of Fe_{0.5}Co_{0.5} at $T = 0$ K and $\mu_{\text{Fe}} = \mu_{\text{Co}}$.

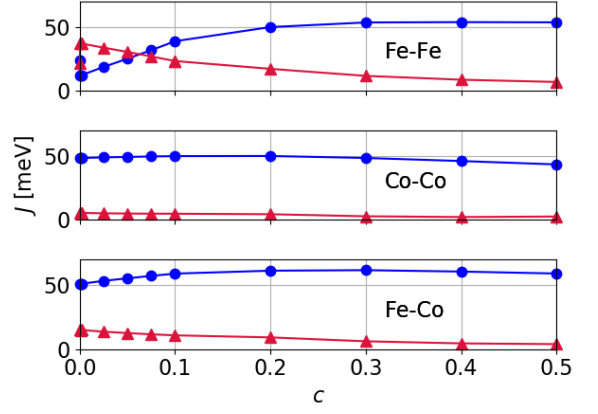


Figure 9. Exchange interaction in iron-cobalt alloys nearest neighbors (blue circles), next nearest neighbors (red triangles). The interaction with atoms in outer shells is comparably weak.

element	site 1	site 2
Fe	1	0.6
Co	0	0.4

Table II. Occupation probabilities for the case of short range order.

FWHM at $\mathbf{k}_1 = (0.1, 0, 0) \frac{1}{a_B}$ and $T = 0$ K for different concentrations compared to the FWHM for the case of fixed interactions.

B. Short range order

Our theory is formulated in the framework of the single-site CPA, which by definition is not able to account for the appearance of short range order or any other correlations between the occupation of different sites. However, through our generalization of the theory to lattices with multiple atoms per unit cell, we are able to include short range order through different occupation probabilities within the unit cell. In this section, we discuss the influence of short range order using a very simple model. Instead of performing the calculations for the primitive unit cell, we choose for the case of an alloy exhibiting short range order the usage of the cubic unit cell with 2 atoms and the occupation probabilities listed in table II. This configuration corresponds to an alloy in which two cobalt atoms never sit next to each other. The results for the case of random disorder and short range order are compared in figure 12. As there are now two basis sites occupied with two elements according to table II, the spectrum now consists of three bands. The main result of this test is the verification that the bandgap remains present in the case of an alloy exhibiting short range order.

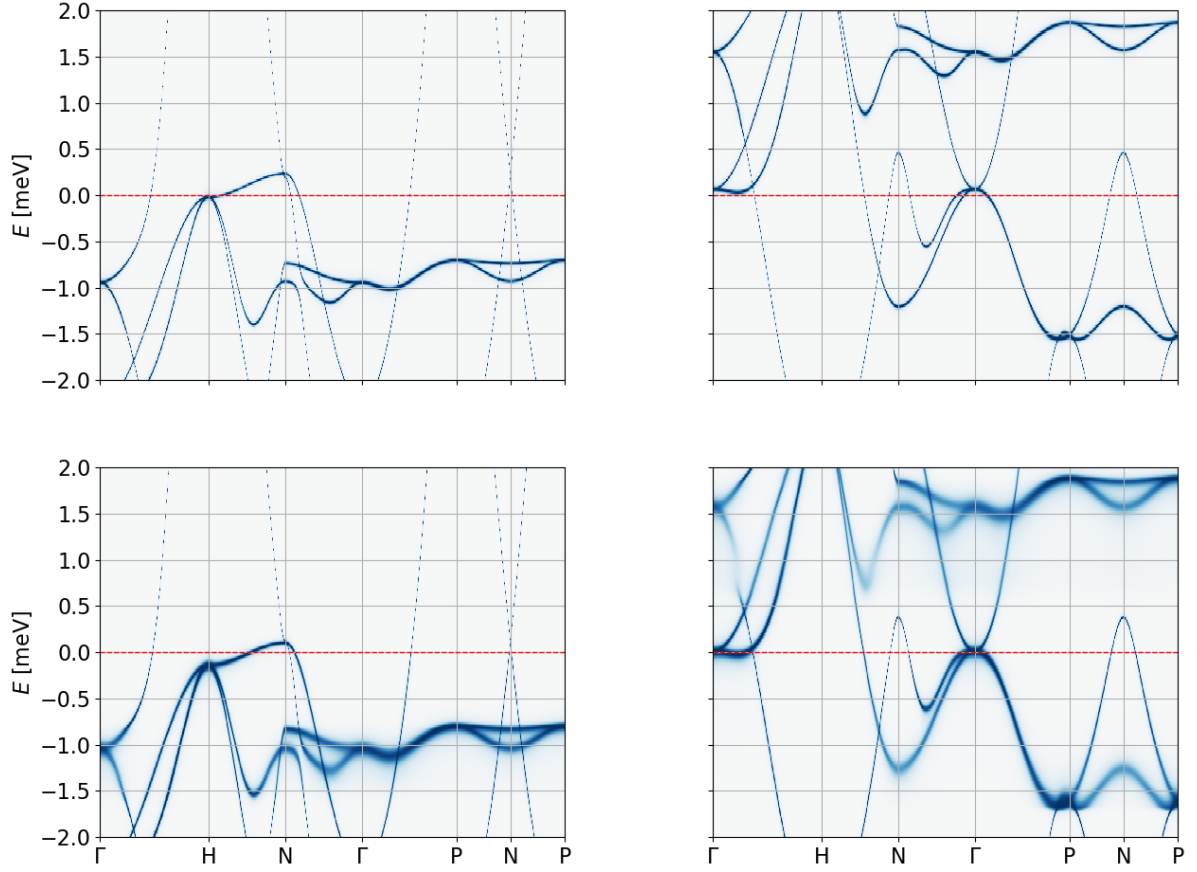


Figure 10. Bloch spectral functions for $\text{Fe}_{0.995}\text{Co}_{0.005}$ (upper panels) and $\text{Fe}_{0.9}\text{Co}_{0.1}$ (lower panels) for majority (left) and minority spin channels, respectively.

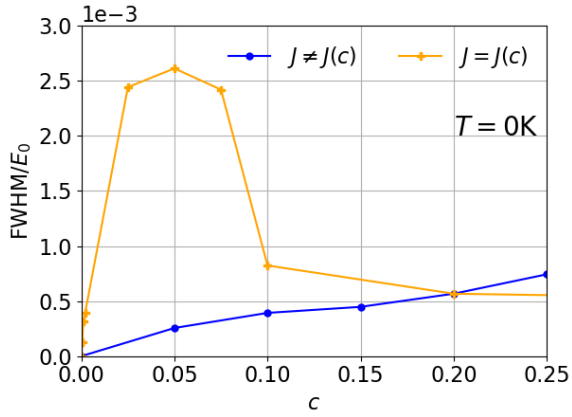


Figure 11. FWHM/E_0 for different concentrations if the interaction parameters are held constant (blue circles) and if they change with the cobalt concentration (orange crosses).

The magnonic properties discussed above in the alloy

with SRO compute to

$$\begin{aligned} E_G &\approx 115\text{meV} \\ \frac{C}{C_0} &= 1.03 \\ \frac{\text{FWHM}}{\text{FWHM}_0} &= 1.92. \end{aligned} \quad (37)$$

It can be seen that the width of the bandgap and the spin stiffness hardly change at all, but the FWHM nearly doubles its value. Obviously, this is far from a complete study of the influence of SRO, but it suggests that the inclusion of SRO will only have a minor impact on the width of the bandgap.

V. SUMMARY

We presented a first-principle approach to calculate critical magnetic phenomena and spin waves at finite temperatures for complex disordered materials. The method is based on a mapping of a Green function, obtained within the multiple scattering theory, on the

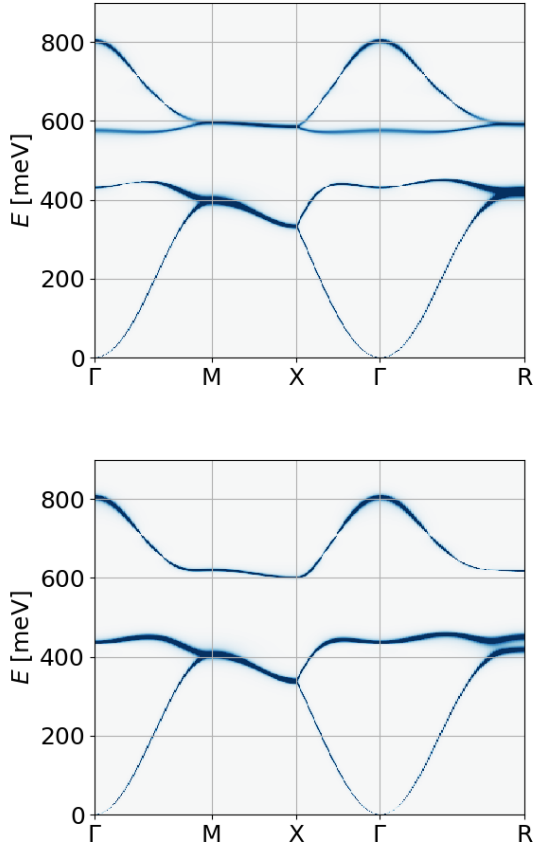


Figure 12. Magnonic spectrum of $\text{Fe}_{0.8}\text{Co}_{0.2}$ with random disorder (top), and in a configuration in which all cobalt atoms are isolated from each other according to the occupation probabilities given in table II at $T = 0$ K (bottom).

Heisenberg model using a coherent potential approximation. The temperature effects were taken into account within an RPA for the magnonic Green function.

Our approach is illustrated on disordered iron-cobalt alloys which exhibit many of the properties demanded from magnonic crystals: They exhibit a bandgap whose width shows an interesting behavior in the concentration and temperature range studied in this work. The influence of short range order on the bandgap turns out to be of minor importance in our calculations. However, the latter result should only be seen as an intermediate step obtained for one specific type of SRO and needs further investigation.

The temperature dependence of the bandwidth and the spin stiffness mirrors the decreasing magnetization as the temperature is increased. Thus the treatment of temperature is far from complete. Moreover, the inclusion of Landau damping in the description of disordered systems is a further necessary improvement of the theory which we currently develop.

-
- [1] A. V. Chumak, V. I. Vasyuchka, A. A. Serga, and B. Hillebrands, Magnon spintronics, *Nature Physics* **11**, 453 (2015).
 - [2] A. Khitun and K. L. Wang, Non-volatile magnonic logic circuits engineering, *Journal of Applied Physics* **110**, 034306 (2011).
 - [3] H. Al-Wahsh, A. Akjouj, B. Djafari-Rouhani, and L. Dobrzynski, Magnonic circuits and crystals, *Surface Science Reports* **66**, 29 (2011).
 - [4] F. Bloch, Zur theorie des ferromagnetismus, *Zeitschrift für Physik* **61**, 206 (1930).
 - [5] A. V. Chumak, A. A. Serga, and B. Hillebrands, Magnonic crystals for data processing, *Journal of Physics D: Applied Physics* **50**, 244001 (2017).
 - [6] S. Nikitov, P. Tailhades, and C. Tsai, Spin waves in periodic magnetic structures—magnonic crystals, *Journal of Magnetism and Magnetic Materials* **236**, 320 (2001).
 - [7] M. Krawczyk and D. Grundler, Review and prospects of magnonic crystals and devices with reprogrammable band structure, *Journal of Physics: Condensed Matter* **26**, 123202 (2014).
 - [8] B. Lenk, H. Ulrichs, F. Garbs, and M. Münzenberg, The building blocks of magnonics, *Physics Reports* **507**, 107 (2011).
 - [9] A. V. Sadovnikov, E. N. Beginin, S. A. Odincov, S. E. Sheshukova, Y. P. Sharaevskii, A. I. Stognij, and S. A. Nikitov, Frequency selective tunable spin wave channeling in the magnonic network, *Applied Physics Letters* **108**, 172411 (2016).
 - [10] A. Sadovnikov, V. Gubanov, S. Sheshukova, Y. Sharaevskii, and S. Nikitov, Spin-wave drop filter based on asymmetric side-coupled magnonic crystals, *Physical Review Applied* **9**, 10.1103/physrevapplied.9.051002 (2018).
 - [11] S. E. Sheshukova, M. A. Morozova, E. N. Beginin, Y. P. Sharaevskii, and S. A. Nikitov, Formation of gap solitons in a finite magnonic crystal, *Physics of Wave Phenomena* **21**, 304 (2013).
 - [12] K. Zakeri, Terahertz magnonics: Feasibility of using terahertz magnons for information processing, *Physica C: Superconductivity and its Applications* **549**, 164 (2018).
 - [13] P. Buczek, A. Ernst, and L. M. Sandratskii, Stand-

- ing spin waves as a basis for the control of terahertz spin dynamics: Time dependent density functional theory study, *Physical Review Letters* **105**, 10.1103/physrevlett.105.097205 (2010).
- [14] P. Buczek, A. Ernst, P. Bruno, and L. M. Sandratskii, Energies and lifetimes of magnons in complex ferromagnets: A first-principle study of heusler alloys, *Physical Review Letters* **102**, 10.1103/physrevlett.102.247206 (2009).
 - [15] A. S. Normanton, P. E. Bloomfield, F. R. Sale, and B. B. Argent, A calorimetric study of iron-cobalt alloys, *Metal Science* **9**, 510 (1975).
 - [16] T. Nishizawa and K. Ishida, The co-fe (cobalt-iron) system, *Bulletin of Alloy Phase Diagrams* **5**, 250 (1984).
 - [17] P. Buczek, A. Ernst, and L. M. Sandratskii, Interface electronic complexes and landau damping of magnons in ultrathin magnets, *Physical Review Letters* **106**, 10.1103/physrevlett.106.157204 (2011).
 - [18] P. Buczek, A. Ernst, and L. M. Sandratskii, Different dimensionality trends in the landau damping of magnons in iron, cobalt, and nickel: Time-dependent density functional study, *Physical Review B* **84**, 10.1103/physrevb.84.174418 (2011).
 - [19] K. Zakeri, Y. Zhang, T.-H. Chuang, and J. Kirschner, Magnon lifetimes on the fe(110) surface: The role of spin-orbit coupling, *Physical Review Letters* **108**, 10.1103/physrevlett.108.197205 (2012).
 - [20] H. J. Qin, K. Zakeri, A. Ernst, L. M. Sandratskii, P. Buczek, A. Marmodoro, T. H. Chuang, Y. Zhang, and J. Kirschner, Long-living terahertz magnons in ultrathin metallic ferromagnets, *Nature Communications* **6**, 10.1038/ncomms7126 (2015).
 - [21] P. Buczek, L. M. Sandratskii, N. Buczek, S. Thomas, G. Vignale, and A. Ernst, Magnons in disordered nonstoichiometric low-dimensional magnets, *Physical Review B* **94**, 10.1103/physrevb.94.054407 (2016).
 - [22] P. Buczek, S. Thomas, A. Marmodoro, N. Buczek, X. Zubizarreta, M. Hoffmann, T. Balashov, W. Wulfhekkel, K. Zakeri, and A. Ernst, Spin waves in disordered materials, *Journal of Physics: Condensed Matter* **30**, 423001 (2018).
 - [23] H. B. Callen, Green function theory of ferromagnetism, *Physical Review* **130**, 890 (1963).
 - [24] E. Şaşıoğlu, C. Friedrich, and S. Blügel, Strong magnon softening in tetragonal FeCo compounds, *Physical Review B* **87**, 10.1103/physrevb.87.020410 (2013).
 - [25] A. Liechtenstein, M. Katsnelson, V. Antropov, and V. Gubanov, Local spin density functional approach to the theory of exchange interactions in ferromagnetic metals and alloys, *Journal of Magnetism and Magnetic Materials* **67**, 65 (1987).
 - [26] W. Nolting and A. Ramakanth, *Quantum Theory of Magnetism* (Springer, 2009).
 - [27] F. Yonezawa, A systematic approach to the problems of random lattices. i: A self-contained first-order approximation taking into account the exclusion effect, *Progress of Theoretical Physics* **40**, 734 (1968).
 - [28] T. Matsubara, An application of CPA to a random spin system, *Progress of Theoretical Physics Supplement* **53**, 202 (1973).
 - [29] G. X. Tang and W. Nolting, Magnetic properties of disordered heisenberg binary spin system with long-range exchange, *Physical Review B* **73**, 10.1103/physrevb.73.024415 (2006).
 - [30] G. Bouzerar and P. Bruno, RPA-CPA theory for magnetism in disordered heisenberg binary systems with long-range exchange integrals, *Physical Review B* **66**, 10.1103/physrevb.66.014410 (2002).
 - [31] J. Ruzs, I. Turek, and M. Diviš, Random-phase approximation for critical temperatures of collinear magnets with multiple sublattices: GdX compounds (x=mg, rh, ni, pd), *Physical Review B* **71**, 10.1103/physrevb.71.174408 (2005).
 - [32] P. E. Blöchl, O. Jepsen, and O. K. Andersen, Improved tetrahedron method for brillouin-zone integrations, *Physical Review B* **49**, 16223 (1994).
 - [33] S. Geršgorin, Über die Abgrenzung der Eigenwerte einer Matrix, *Bulletin de l'Académie des Sciences de l'URSS* (1931).
 - [34] J. P. Perdew, K. Burke, and M. Ernzerhof, Generalized gradient approximation made simple, *Physical Review Letters* **77**, 3865 (1996).
 - [35] M. Lüders, A. Ernst, W. M. Temmerman, Z. Szotek, and P. J. Durham, Ab initio angle-resolved photoemission in multiple-scattering formulation, *Journal of Physics: Condensed Matter* **13**, 8587 (2001).
 - [36] M. Geilhufe, S. Achilles, M. A. Köbis, M. Arnold, I. Mertig, W. Hergert, and A. Ernst, Numerical solution of the relativistic single-site scattering problem for the coulomb and the mathieu potential, *Journal of Physics: Condensed Matter* **27**, 435202 (2015).
 - [37] M. Hoffmann, A. Ernst, W. Hergert, V. N. Antonov, W. A. Adeagbo, R. M. Geilhufe, and H. B. Hamed, Magnetic and electronic properties of complex oxides from first-principles, *physica status solidi (b)* **257**, 1900671 (2020), <https://onlinelibrary.wiley.com/doi/pdf/10.1002/pssb.201900671>.
 - [38] P. Soven, Coherent-potential model of substitutional disordered alloys, *Physical Review* **156**, 809 (1967).
 - [39] B. L. Gyorffy, Coherent-potential approximation for a nonoverlapping-muffin-tin-potential model of random substitutional alloys, *Physical Review B* **5**, 2382 (1972).
 - [40] I. Turek, J. Kudrnovský, V. Drchal, and P. Bruno, Exchange interactions, spin waves, and transition temperatures in itinerant magnets, *Philosophical Magazine* **86**, 1713 (2006).
 - [41] E. Kokorina and M. Medvedev, Magnetization and magnetic entropy change of a three-dimensional isotropic ferromagnet near the curie temperature in the random phase approximation, *Physica B: Condensed Matter* **416**, 29 (2013).
 - [42] F. Essenberg, P. Buczek, A. Ernst, L. Sandratskii, and E. K. U. Gross, Paramagnons in FeSe close to a magnetic quantum phase transition: ab initio study, *Physical Review B* **86**, 10.1103/physrevb.86.060412 (2012).
 - [43] K. Hüller, The spin wave excitations and the temperature dependence of the magnetization in iron, cobalt, nickel and their alloys, *Journal of Magnetism and Magnetic Materials* **61**, 347 (1986).
 - [44] P. Knoll, C. Thomsen, M. Cardona, and P. Murugaraj, Temperature-dependent lifetime of spin excitations in R₂Ba₂Cu₃O₆ (r=eu, y), *Physical Review B* **42**, 4842 (1990).